Explorations of water oxidation catalysis in explicit solvent

Ruiter, J.M. de

General Introduction & Computational Tools

Chapter One

1. General Introduction and Computational Tools

Abstract

In this chapter the context for this thesis is introduced. Furthermore a brief outline is given of the computational methods used, as well as supporting theory.

1.1. The search for sustainable energy solutions

World-wide, there is an increasing amount of attention being invested into sustainable energy solutions,[1–3] one of which is hydrogen. A critical hurdle is securing a sustainable supply of hydrogen.[4] Not only can hydrogen replace fossil fuels as a combustible source of energy, it is an essential part of the Haber-Bosch process, and plays an important role in carbon chemistry. The Haber-Bosch process uses hydrogen to produce ammonia which, as an agricultural fertilizer, is responsible for food production for a significant percentage of the global population.[5] Indeed, around half of the hydrogen produced globally is used for ammonia production.[6,7] As the global population increases, the need for food, and therefore hydrogen, must surely increase. Furthermore, unprecedented amounts of hydrogen will be needed within the chemical industry: hydrogen can be reacted with CO_2, both from the atmosphere as well as from industrial emissions, to produce useable hydrocarbons. However, this must occur on the gigatonne scale.[8] Considering that around 95 % of hydrogen is currently generated via steam reforming of natural gas,[6,7] new hydrogen generation methods must be explored.

One of the most promising methods of generating hydrogen is via artificial photosynthesis. A schematic representation of an artificial photosynthetic system is shown in Figure 1.1.[9] An antenna component absorbs sunlight which is used to excite an electron in the photosensitiser, after which excitation energy is converted into electrochemical energy. This electrochemical energy is used as redox potential by a WOC to catalyse water splitting. This splitting results in oxygen, hydrogen ions, and electrons which are stored as reducing equivalents. These reducing equivalents are then transferred via an electron transfer system

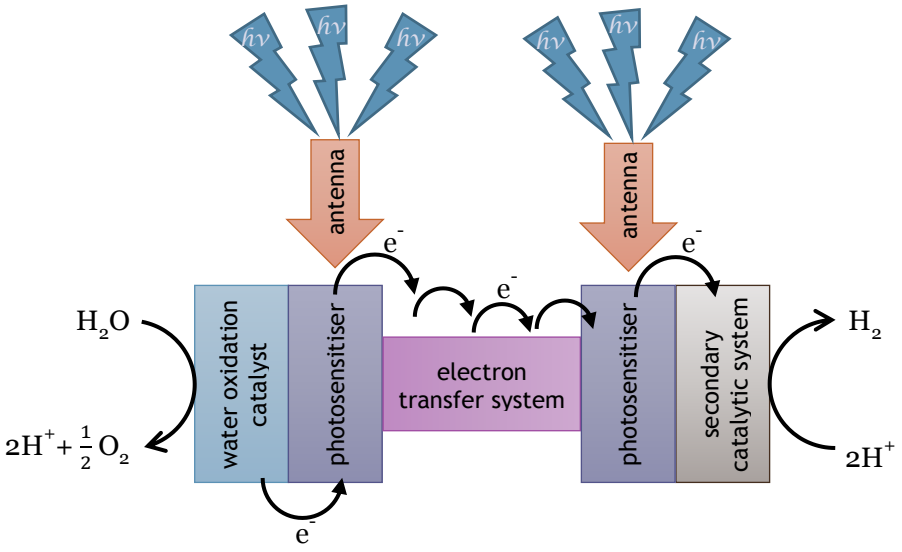

Figure 1.1 The basic components of a solar fuel production system

and a second photosensitiser to a secondary catalytic system which then reduces the hydrogen ions to molecular hydrogen. This secondary catalytic system may also be used in the generation of hydrocarbons. Although this may sound straight forward, challenges include rapid and efficient water splitting, efficient visible-light absorption and stable charge separation.[10] Stable charge separation is one of the greatest challenges, which the natural photosynthetic system achieves by means of a highly complex electron transfer system that prevents back reactions

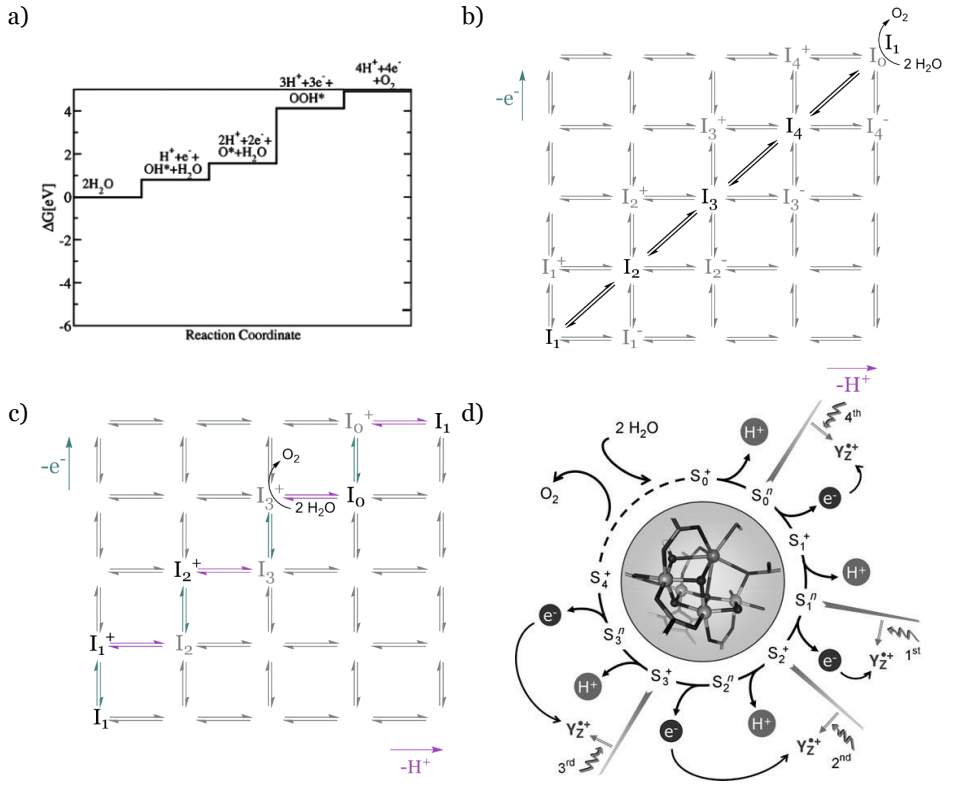

Figure 1.2 (a) The changes in free energy for the four PCET steps of a heterogeneous WOC, where * indicates the adsorbents. Adapted from Rossmeisl et al.[22] (b) The four PCET steps between the catalytic intermediates I_1 - I_0. Vertical lines denote electron transfer, horizontal lines proton transfer. The ligand exchange $I_0 + H_2O \rightarrow I_1 + O_2$ is shown in the top right corner. (c) The decoupled PCET reactions of the Mn complex, where vertical lines denote electron transfer and horizontal lines proton transfer. The stable states are shown in black: I_1, I_1^+, I_2^+ and I_0, which correspond to S_1^n, S_2^+, S_3^+ and S_0^n in Dau's notation shown in (d). (d) The water oxidation mechanism for the Mn complex in the natural photosynthetic system, as reproduced from Dau et al.[19] We note that two of the stable states shown in (c) are off-diagonal when compared to (b), these represent the interchange of transition states and intermediates. The start of the cycle (I_0, I_1) has intermediates on the diagonal, while the I_1^+ and I_2^+ are off-diagonal. This leads to a mismatch between the end and the start of the reaction coordinate that requires a rearrangement involving the exchange of O_2 by $2H_2O$ in an energetically downhill process. This supplies a molecular level heat pulse at the right time and location for the release of the gaseous O_2.

and electron-hole recombination, by matching time, length and energy scales.[11]

Water splitting forms an important challenge in the move towards a fully sustainable energy infrastructure,[12–14] which has led to an explosion in the WOC research field.[10,15–18] The primary function of a WOC is to drive water oxidation. To do so, it must be able to process four electrons, according to

$$2H_2O \rightarrow O_2 + 4H^+ + 4e^-. \qquad (1.1)$$

The thermodynamic potential E^0 of water oxidation is 1.23 V. In the natural photosynthetic system this reaction proceeds via PCET steps.[19] The water oxidation mechanism for many heterogeneous catalysts also features four PCET steps. The pH-independent changes in free energy throughout the catalytic cycle are often depicted as shown in Figure 1.2 (a). Although at longer time scales one might consider these steps concerted, i.e. that proton and electron transfer occurs simultaneously, on short enough timescales these processes will be decoupled. If we consider Figure 1.2 (b), the diagonal arrows would denote the concerted reaction. If we were to decouple the electron and proton transfer processes, proton and electron transfer could occur in varying sequences throughout the catalytic cycle. For example, one could first transfer one electron ($I_1 \rightarrow I_1^+$) in Figure 1.2 (b) followed by two protons ($I_1^+ \rightarrow I_2^-$). This technique is also employed in the natural photosynthetic system, as shown in Figure 1.2 (c), yielding a total of 9 decoupled states (Figure 1.2 (d)),[20] in contrast to the four intermediates S0-S3 of the Kok model.[21] Though the second step is PCET, the first catalytic step involves only the transfer of an electron ($I_1 \rightarrow I_1^+$ in Figure 1.2 (c)). These sequences could therefore be modified in the search for an optimal water oxidation catalyst.

In the search for the optimal water oxidation catalyst, one should bear in mind the energetic relationships between catalytic intermediates. It has been established, using heterogeneous catalysis, that a scaling relationship exists between the adsorption energies of the OH and OOH groups (see Figure 1.3, left).[23,24] Because the OH and OOH groups bind to surfaces in similar ways, the stabilisation or destabilisation of one intermediate will affect the other in the same way. For various oxide surfaces the difference in energies between the OH and OOH intermediates remains roughly constant at 3.2 eV.[24] This introduces a minimum overpotential for WOCs, where the overpotential is the difference between the potential at which a WOC operates and 1.23 V. Plotting negative overpotential as a function of the descriptor $\Delta G_O^0 - \Delta G_{OH}^0$ yields a volcano plot (see Figure 1.3, right), which can be used to evaluate WOCs. The apex of the volcano indicates the minimum overpotential needed to overcome both O and OH binding energies.[24]

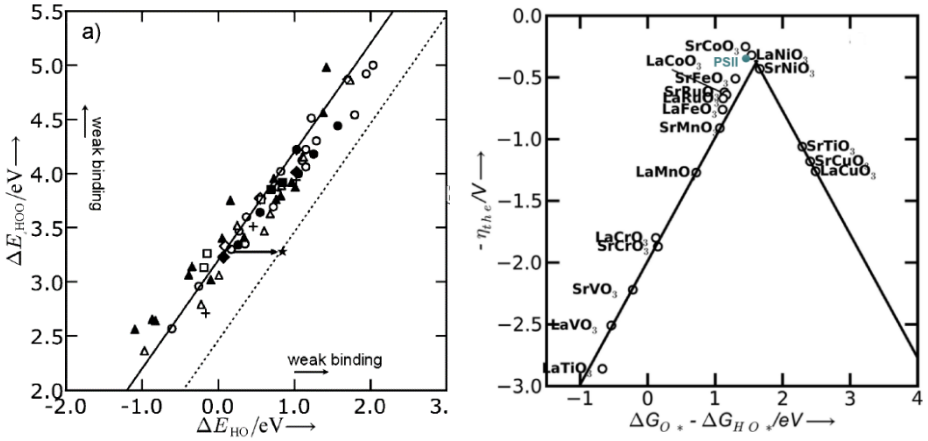

Figure 1.3 (left) Adsorption energy of OOH plotted against the adsorption energy of OH on perovskites, rutiles, anatase, Mn_xO_y, Co_3O_4, and NiO oxides. (right) Activity trends towards oxygen evolution plotted for perovskites. Both reproduced from Man et al., [24] where the PS II data point in (right) has been added (in green) for this thesis.

In designing a biomimetic WOC, there are two energetic properties that should be aimed for. The first is to have differences in energy between catalytic intermediates that would place the WOC on the apex of the volcano plot shown in Figure 1.3 (right). The second is to design the WOC so that intermediates occupy both diagonal and off-diagonal positions when considering the four PCET steps as shown in Figure 1.2 (c). In addressing these challenges, computational techniques will prove essential.

Computational techniques are increasingly employed to test the energetic properties of proposed WOCs.[25–31] Traditionally, catalytic cycles are examined computationally by comparing the free energies of the proposed catalytic intermediates and then, usually, assigning the thermodynamically most favourable cycle as the most likely catalytic cycle.[25–30] This examination often uses an implicit solvent model or correction factors to account for protons and electrons removed in the catalytic step itself.[25,27,29,32–35] Using correction factors prevents direct comparisons of the energy of intermediates as the compared intermediates usually contain different numbers of protons and electrons. In the case of PCET processes,[36] it is also becoming increasingly clear that explicit solvent molecules are needed to obtain realistic descriptions of reaction pathways.[37–39]

The aim of this thesis has been to further examine the catalytic mechanisms of WOCs within an explicit solvent environment, to compare this to the status quo, and to propose a novel approach with which to explore the reaction process and free-energy profile from one catalytic intermediate to the next.

1.2. Computational Tools

1.2.1. Density Functional Theory

The BOA arises from the large mass difference between electrons and nuclei. Electrons usually move much faster than nuclei, so may be considered to readjust instantaneously to changes in nuclear configuration. In this way nuclear and electronic motion may be considered independently from each other. The electronic ground-state can then be studied with DFT. DFT is a well-established computational method which obtains the electronic energy as a functional of the density $\rho(\boldsymbol{r})$ of electrons in the system. We consider a system of N nuclei and n electrons, where the Kth nucleus is positioned at $\boldsymbol{R}_K$ and the ith electron at $\boldsymbol{r}_i$. KS orbitals $\varphi_i(\boldsymbol{r})$, being one-electron wave functions, may be used to obtain the density of the non-interacting system

$$\rho_S(\boldsymbol{r}) = \sum_{i=1}^{n} |\varphi_i(\boldsymbol{r})|^2, \tag{1.2}$$

in atomic units. In atomic units the physical quantities $(4\pi\varepsilon_0)^{-1}$, known as Coulomb's constant with ε_0 the vacuum permittivity; m_e, the mass of an electron; e, the elementary charge; and $\hbar$, the reduced Planck's constant are defined to be 1.

The energy functional

$$\begin{aligned} E &= E[\rho(\boldsymbol{r})] \\ &= T[\rho] + V[\rho] \\ &= T[\rho] + V_{e-e}[\rho] + V_{n-e}[\rho] + V_{n-n}[\rho], \end{aligned} \tag{1.3}$$

includes a kinetic energy term, $T[\rho]$, and a potential term $V[\rho]$ which has three contributions. The potential due to nuclear electron interactions $V_{n-e}[\rho]$ can be generalised to the potential due to an external field, as integrated over all space $\mathbb{R}^3$,

$$V_{n-e}[\rho] = \int_{\mathbb{R}^3} \rho(\boldsymbol{r}) v_{ext}(\boldsymbol{r}) d\boldsymbol{r}, \tag{1.4}$$

which depends solely on changes in geometry. The potential due to nuclear interactions $V_{n-n}[\rho]$, with Z_J the atomic charge of nucleus J

$$V_{n-n}[\rho] = \sum_{J=1,K>J}^{N} \frac{Z_J Z_K}{|\boldsymbol{R}_J - \boldsymbol{R}_K|}, \tag{1.5}$$

is constant for a given nuclear conformation, within the BOA.

$T[\rho]$ and $V_{e-e}[\rho]$ are dependent on the electrons in the system and therefore are universal functionals once the number of electrons is fixed. In

$$T[\rho] + V_{e-e}[\rho] = -\frac{1}{2}\sum_{i=1}^{n}\langle\varphi_i^*|\nabla^2|\varphi_i\rangle + \frac{1}{2}\int_{\mathbb{R}^3}\frac{\rho(\boldsymbol{r})\rho(\boldsymbol{r}')}{|\boldsymbol{r}-\boldsymbol{r}'|}d\boldsymbol{r}d\boldsymbol{r}' + E_{xc}[\rho], \tag{1.6}$$

part of $T[\rho]$ is approximated using the one-electron kinetic energy operator and part of $V_{e-e}[\rho]$ is described by the classical average Coulomb interactions, but the quantum contributions due to electron – electron correlation are still not well described. These unknown terms are collected in the exchange correlation energy functional $E_{xc}[\rho]$ and it is this term that DFT tries to approximate. If $E_{xc}[\rho]$ was given exactly, the KS equations

$$\hat{h}_i^{KS}\varphi_i = \varepsilon_i\varphi_i \tag{1.7}$$

$$\hat{h}_i^{KS} = -\frac{1}{2}\nabla^2 + v_{ext}(\boldsymbol{r}) + \int_{\mathbb{R}^3}\frac{\rho(\boldsymbol{r}')}{|\boldsymbol{r}-\boldsymbol{r}'|}d\boldsymbol{r}' + V_{xc}[\rho] \tag{1.8}$$

would give the exact ground state energy. In Eqn. (1.8) the term V_{xc} is the functional derivative of E_{xc}:

$$V_{xc}[\rho] = \frac{\delta E_{xc}}{\delta\rho}. \tag{1.9}$$

Functionals, basis sets, and other approximations

There are a number of different ways to approximate the $E_{xc}[\rho]$ term, which are then implemented in a variety of different functionals. GGA approximates $E_{xc}[\rho]$ per electron as a function of the electron density ρ as well as the first derivative of the density

$$E_{xc}^{GGA}[\rho,\nabla\rho] = \int_{\mathbb{R}^3}\rho(\boldsymbol{r})f[\rho(\boldsymbol{r}),\nabla\rho(\boldsymbol{r})]\,d\boldsymbol{r}. \tag{1.10}$$

The GGA functional which is primarily used in this thesis is OPBE.[40]

Hybrid GGA functionals

$$E_{xc}^{Hybrid}[\rho] = (1-a)E_{xc}^{GGA}[\rho,\nabla\rho] + aE_{x}^{HF}[\rho], \qquad (1.11)$$

are very widely used. They include part of the exact HF exchange $E_x^{HF}[\rho]$ as well as GGA exchange-correlation $E_{xc}^{GGA}[\rho]$, where a determines the mixing between the HF and GGA exchange. Incorporating HF as well as GGA exchange has been shown to improve the accuracy of a number of molecular properties.[41] Here we use the B3LYP functional which has 20% HF exchange.[42]

The KS orbitals are usually written in terms of a linear combination of basis set functions. Especially in the case of plane wave basis sets, it is customary to use a pseudopotential, which describes the core, or non-valence, electrons of an atom using an effective potential.[43,44] In Gaussian 09 LanL2DZ is used,[45–47] which is a popular pseudopotential for the larger transition metals.[41] In ADF [48–50] Slater-Type Orbitals are used as basis functions. The basis set used, TZP, describes the core electrons using double-zeta, valence electrons using triple-zeta, and includes one polarisation function. This is considered the best balance between accuracy and computational cost for the systems we consider. In CPMD,[51] which uses a plane wave/pseudopotential implementation of DFT, PBE pseudopotentials of the Kleinman-Bylander form are used.[52,53]

Dispersion corrections by Grimme are also added.[54] This attempts to approximate, and correct for, the effect of van der Waals forces (including instantaneous dipole – instantaneous dipole interactions) in the system.

There are two different methods that are used to simulate the solvation of the system in static calculations: in ADF the COSMO,[55] and in Gaussian 09 the PCM.[56] Both methods, though having slightly different origins, currently have similar implementations.[55] The solute molecule is located inside a molecule-shaped cavity within a dielectric medium where the dielectric constant is dependent on the solvent used.

1.2.2. Time Dependent Density Functional Theory

Electronic excited-states are not easily accessible by DFT, which is a ground-state theory in its original formulation. TDDFT is a theory which generalises DFT in the presence of a time-dependent external field.[57–61] Here we focus on linear response TDDFT in particular, which makes use of the KS orbitals obtained in the ground-state. If we consider an excitation induced by a perturbation due to a time-dependent external potential $\delta v_{ext}(\boldsymbol{r},t)$, linear response theory applies when this perturbation is sufficiently small. The density response depends on perturbations at other positions $\boldsymbol{r}'$ and earlier times t'. Time t is replaced by

frequency ω in order to facilitate the extraction of the excitation energies from the linear response of the system.[61]

The first order change in density

$$\delta\rho(\boldsymbol{r},\omega) = \int_{\mathbb{R}^3} \chi_s(\boldsymbol{r},\boldsymbol{r}';\omega)\, \delta v_{eff}(\boldsymbol{r}',\omega)\, d\boldsymbol{r}', \tag{1.12}$$

features the response function of the non-interacting KS system,

$$\chi_s(\boldsymbol{r},\boldsymbol{r}';\omega) = \sum_{i=1}^{n}\sum_{a=1}^{m} 2\frac{\omega_{ai}}{\omega^2-\omega_{ai}^2}\varphi_i(\boldsymbol{r})\varphi_a(\boldsymbol{r})\varphi_i(\boldsymbol{r}')\varphi_a(\boldsymbol{r}'). \tag{1.13}$$

$\chi_s(\boldsymbol{r},\boldsymbol{r}';\omega)$ depends on the unperturbed KS orbitals $\varphi_i(\boldsymbol{r})$ and the difference in energy eigenvalues $\omega_{ai} \equiv \varepsilon_a - \varepsilon_i$ of the virtual $\varphi_a(\boldsymbol{r})$ and occupied $\varphi_i(\boldsymbol{r})$ KS orbitals, both of which may be obtained from the initial DFT calculation. Furthermore, $\chi_s(\boldsymbol{r},\boldsymbol{r}';\omega)$ has poles at the excitation energies of the KS system.

$\delta\rho(\boldsymbol{r},\omega)$ also contains the perturbation of the effective potential

$$\delta v_{eff}(\boldsymbol{r}',\omega) = \int_{\mathbb{R}^3} \frac{\delta\rho(\boldsymbol{r}',\omega)}{|\boldsymbol{r}-\boldsymbol{r}'|} d\boldsymbol{r}' + \delta v_{ext}(\boldsymbol{r},\omega) + \delta v_{xc}(\boldsymbol{r},\omega), \tag{1.14}$$

which depends on the two terms $\delta\rho(\boldsymbol{r},\omega)$ and $\delta v_{ext}(\boldsymbol{r},\omega)$, as well as the linearised exchange correlation potential

$$\delta v_{xc}(\boldsymbol{r},\omega) = \int_{\mathbb{R}^3} f_{xc}(\boldsymbol{r},\boldsymbol{r}';\omega)\, \delta\rho(\boldsymbol{r},\omega)\, d\boldsymbol{r}'. \tag{1.15}$$

$\delta v_{xc}(\boldsymbol{r},\omega)$ contains the time-dependent exchange correlation kernel

$$f_{xc}(\boldsymbol{r},\boldsymbol{r}';\omega) = \left.\frac{\delta v_{xc}(\boldsymbol{r},\omega)}{\delta\rho(\boldsymbol{r}',\omega)}\right|_{\rho=\rho_0}, \tag{1.16}$$

the functional derivative being computed at the ground state density ρ_0. $f_{xc}(\boldsymbol{r},\boldsymbol{r}';\omega)$ is responsible, along with the self-consistency of Eqn. (1.12) and (1.14), for the shifting of the KS poles to the exact excitation energies. The approximation of f_{xc} should technically be linked to the approximation used for

the ground-state xc potential. However, in quantum chemistry codes they are often treated independently. In this thesis the ALDA kernel

$$f_{xc}^{ALDA}(\boldsymbol{r},\boldsymbol{r}';\omega) = \delta(\boldsymbol{r}-\boldsymbol{r}')\frac{d^2}{d\rho^2}(\rho\cdot\varepsilon_{xc}(\rho))\Big|_{\rho=\rho_0} \tag{1.17}$$

is applied,[60] where for $\varepsilon_{xc}(\rho)$, the exchange correlation energy density, a parameterisation of a homogenous electron gas is used.

1.2.3. Car-Parrinello Molecular Dynamics

MD is an established method of investigating the dynamics in a system. In MD it is assumed that the nuclei are heavy enough to be described by classical mechanics and so Newton's equations of motion are used. The forces used in the evolution of the system are often derived by an effective potential, usually called a force field, containing empirical parameters, which is a severe limitation of the MD method. As a result, not all molecules will be well described due to the transferability problem, and the breaking and making of bonds cannot be simulated. The transferability problem describes the inability of force fields that have been optimised for one class of systems to be transferred to a different class of systems.

In an attempt to ameliorate this, AIMD has been developed, where the forces are calculated at each time step by solving the electronic structure for the nuclear configuration at that point in the trajectory. However, this can be computationally very demanding. In response to this, CPMD forms an approach in which the electronic structure is only solved for the initial configuration, and then evolved in time using an extended Lagrangian.[62,63] The evolved electronic structure then provides the forces needed to drive the nuclear dynamics. As a result, the nuclear trajectory and its corresponding electronic ground state are calculated simultaneously, which is significantly less computationally expensive. Usually the electronic structure problem within AIMD is solved using DFT, since this achieves the best compromise between accuracy and computational effort. The Euler-Lagrange equations of motions are given by

$$M_I\frac{d^2}{dt^2}\boldsymbol{R}_I = -\nabla_I E[\boldsymbol{R},\varphi] \tag{1.18}$$

for the dynamics of the nuclei with mass M, and

$$\mu\frac{d^2}{dt^2}\varphi_i = -\frac{\delta E}{\delta\varphi_i} + \sum_j \lambda_{ij}\varphi_j \tag{1.19}$$

for the evolution of the electrons, where μ is the fictitious electron mass, λ_{ij} the

Lagrange multipliers associated to the orthonormalisation condition of the KS orbitals φ_i, and E is the density functional as per Eqn. (1.3).

1.2.4. Calculating changes in Relative Free Energies

Changes in free energy calculated using static calculations

The Gibbs free energy difference, as considered using static calculations, between each catalytic intermediate is calculated following the method first proposed by Norskov and co-workers.[22,64,65] The structures of the intermediates are optimised in vacuum. The zero-point energy and entropic contributions are included through vibrational analysis performed with the same computational set-up. For every structure optimised in vacuum, solvation effects are accounted for by performing a single point calculation in a water environment simulated with the COSMO model to give E_{solv}. Enthalpies E, zero-point energies ZPE and entropies S of O_2, H_2 and H_2O are also calculated in this manner. Furthermore, as the catalytic cycle proceeds via PCET steps, the free energy of the proton and electron are calculated as a pair: $H^+ + e^- \rightarrow \frac{1}{2} H_2$.

In other words, considering that

$$\Delta G = \Delta E - T\Delta S + \Delta ZPE \tag{1.20}$$

and, because ZPE calculations are more consistently achievable in vacuum, G is approximated by

$$\begin{aligned} G &= (E_{vac} + ZPE_{vac} - TS_{vac}) + \delta E_{solv}, \\ \delta E_{solv} &= E_{solv} - E_{vac}. \end{aligned} \tag{1.21}$$

Then for the first PCET reaction step in Figure 1.2 (b)

$$I_i \longrightarrow I_{i+1} + H^+ + e^-, \tag{1.22}$$

the change in free energy is given by

$$\Delta G(I_i \longrightarrow I_{i+1}) = G(I_{i+1}) - G(I_i) + \Delta G(H^+) + \Delta G(e^-), \tag{1.23}$$

where G is approximated by Eqn. (1.21) and $H^+ + e^-$ by $\frac{1}{2}H_2$.

Using constrained CPMD to calculate changes in free energy

The Gibbs free energy difference, as considered using dynamic calculations, between each catalytic intermediate is calculated following a constrained MD method.[66–68] By constraining a reaction coordinate (in this case the distance

between two atoms) at fixed values along a reaction path, the time-averaged constraint force $\langle\lambda\rangle_x$ for each of these values is obtained. The time-averaged constraint force is equal to zero at an equilibrium or transition state (see Figure 1.4), and it has been shown that $\langle\lambda\rangle$ corresponds to the thermodynamic force $\frac{\partial G}{\partial x}$,[68–70] which may be integrated

$$\int_{x1}^{x2} \langle\lambda\rangle_x \, dx \Rightarrow \Delta G(x1 \rightarrow x2) \qquad (1.24)$$

to give the free energy change along the reaction path.[68–70]

It should be noted that the time-scale of the events observed using this methodology will not be comparable with experiment, though the reaction rate can be extracted using transition state theory.[71]

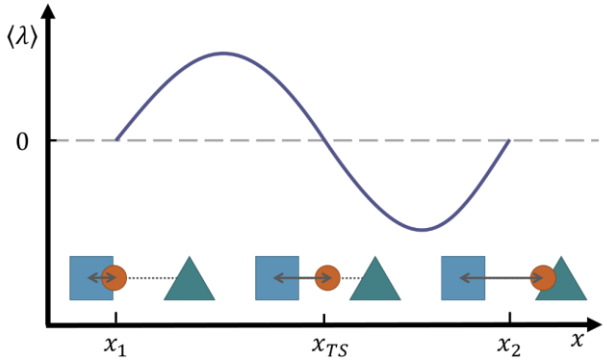

Figure 1.4 The time-averaged constraint force $\langle\lambda\rangle$ as a function of the reaction coordinate x. Here the reaction coordinate is the distance between square and circle as the circle is transferred from the square to the triangle, where x_1 and x_2 are equilibrium states and x_{TS} is the transition state.

1.3. Main Results

The traditional computational methods for establishing a WOC's mechanism are demonstrated in Chapter Two, where a combined experimental and computational analysis is performed on a series of ruthenium-based WOCs. This analysis shows that computational techniques allow for a more in-depth understanding and interpretation of experimental data.

The case for the inclusion of an explicit solvent with regard to mechanistic considerations is given in Chapter Three. There it is observed that including explicit water molecules leads to a different preferred reaction path than would be initially expected by following traditional computational methods. The closed system approach is also introduced, which allows for the decoupling of proton

and electron transfer.

One of the ruthenium-based WOCs investigated in Chapter Two is examined in Chapter Four within an explicit solvent environment including an electron acceptor. Furthermore, the case for a closed system approach is made with regard to energetics. The energetics of the first two catalytic steps are investigated, and taking the energetic contribution of the electron acceptor as constant, these agree with experiment to within 0.1 eV.

Proton diffusion within explicit solvent is further investigated in Chapter Five, where appropriate water wires were observed to facilitate highly rapid proton migration. Furthermore, the inclusion of an OH^- ion as a proton acceptor significantly decreased the thermodynamic barrier of the O – O bond formation step of the earlier investigated ruthenium-based WOC.

1.4. References

[1] B. Christian. "This boat will make its own fuel on a round-the-world voyage" *WIRED UK*. February 20, 2017.
[2] K. Schächtele. "Flying towards a fossil fuel-free future: the HY4 and its plans for zero emission passenger flights" *WIRED UK*. January 12, 2016.
[3] I. Ajjawi *et al. Nat. Biotechnol.* **2017**, *35*, 647–652.
[4] J. O. M. Bockris. *Int. J. Hydrog. Energy* **2013**, *38*, 2579–2588.
[5] J. W. Erisman *et al. Nat. Geosci.* **2008**, *1*, 636–639.
[6] R. Lan *et al. Int. J. Hydrog. Energy* **2012**, *37*, 1482–1494.
[7] N. Armaroli and V. Balzani. *ChemSusChem* **2011**, *4*, 21–36.
[8] A.M. Bazzanella and F. Ausfelder. *Low carbon energy and feedstock for the European chemical industry*; DECHEMA | Gesellschaft für Chemische Technik und Biotechnologie e.V, 2017.
[9] D. Gust *et al. Acc. Chem. Res.* **2009**, *42*, 1890–1898.
[10] K. J. Young *et al. Coord. Chem. Rev.* **2012**, *256*, 2503–2520.
[11] V. W. Lau *et al. Angew. Chem. Int. Ed.* **2017**, *56*, 510–514.
[12] H. L. Tuller. *Mater. Renew. Sustain. Energy* **2017**, *6*, 3.
[13] J. A. Herron *et al. Energy Environ. Sci.* **2015**, *8*, 126–157.
[14] D. Hetterscheid. *Chem. Commun.* **2017**.
[15] J. Hessels *et al. Chem. – Eur. J.* **2017**, *23*, 16413–16418.
[16] P. Garrido-Barros *et al. Chem. Soc. Rev.* **2017**, *46*, 6088–6098.
[17] K. Maeda and K. Domen. *J. Phys. Chem. Lett.* **2010**, *1*, 2655–2661.
[18] A. Thapper *et al. Green* **2013**, *3*, 43–57.
[19] H. Dau *et al. ChemCatChem* **2010**, *2*, 724–761.
[20] H. Dau and M. Haumann. *Biochim. Biophys. Acta BBA - Bioenerg.* **2007**, *1767*, 472–483.
[21] B. Kok *et al. Photochem. Photobiol.* **1970**, *11*, 457–475.
[22] J. Rossmeisl *et al. Chem. Phys.* **2005**, *319*, 178–184.
[23] M. T. M. Koper. *Chem. Sci.* **2013**, *4*, 2710–2723.
[24] I. C. Man *et al. ChemCatChem* **2011**, *3*, 1159–1165.
[25] D. E. Polyansky *et al. J. Am. Chem. Soc.* **2011**, *133*, 14649–14665.
[26] J. D. Blakemore *et al. J. Am. Chem. Soc.* **2010**, *132*, 16017–16029.
[27] T. Wang *et al. J. Chem. Theory Comput.* **2010**, *6*, 2395–2401.
[28] M. D. Kärkäs *et al. Angew. Chem. Int. Ed.* **2012**, *51*, 11589–11593.
[29] A. Venturini *et al. Chem. – Eur. J.* **2014**, *20*, 5358–5368.
[30] M. Orio *et al. Photosynth. Res.* **2009**, *102*, 443–453.

[31] H. A. Younus *et al. ChemSusChem* **2017**, *10*, 862–875.
[32] T. Zhang *et al. J. Am. Chem. Soc.* **2014**, *136*, 273–281.
[33] A. V. Marenich *et al. Angew. Chem. Int. Ed.* **2012**, *51*, 12810–12814.
[34] J. J. Concepcion *et al. J. Am. Chem. Soc.* **2008**, *130*, 16462–16463.
[35] R.-Z. Liao and P. E. M. Siegbahn. *ChemSusChem* **2017**, *10*, 4236–4263.
[36] S. Hammes-Schiffer. *Acc. Chem. Res.* **2009**, *42*, 1881–1889.
[37] C. Ma *et al. ACS Catal.* **2012**, *2*, 1500–1506.
[38] J. L. Vallés-Pardo *et al. ChemPhysChem* **2012**, *13*, 140–146.
[39] T. J. Eisenmayer and F. Buda. *ChemPhysChem* **2014**, *15*, 3258–3263.
[40] M. Swart *et al. Mol. Phys.* **2004**, *102*, 2467–2474.
[41] C. J. Cramer. *Essentials of Computational Chemistry: Theories and Models*; Wiley: Chichester, 2005.
[42] P. J. Stephens *et al. J. Phys. Chem.* **1994**, *98*, 11623–11627.
[43] N. Troullier and J. L. Martins. *Phys. Rev. B* **1991**, *43*, 1993–2006.
[44] O. A. von Lilienfeld *et al. Phys. Rev. Lett.* **2004**, *93*, 153004.
[45] P. J. Hay and W. R. Wadt. *J. Chem. Phys.* **1985**, *82*, 270–283.
[46] P. J. Hay and W. R. Wadt. *J. Chem. Phys.* **1985**, *82*, 299–310.
[47] W. R. Wadt and P. J. Hay. *J. Chem. Phys.* **1985**, *82*, 284–298.
[48] G. te Velde *et al. J. Comput. Chem.* **2001**, *22*, 931–967.
[49] SCM. *ADF 2012*; Theoretical Chemistry, Vrije Universiteit, Amsterdam, The Netherlands.
[50] C. F. Guerra *et al. Theor. Chem. Acc.* **1998**, *99*, 391–403.
[51] *CPMD*; Copyright IBM Corp 1990-2008, Copyright MPI für Festkörperforschung Stuttgart 1997-2001.
[52] I.-C. Lin *et al. Phys. Rev. B* **2007**, *75*, 205131.
[53] L. Kleinman and D. M. Bylander. *Phys. Rev. Lett.* **1982**, *48*, 1425–1428.
[54] S. Grimme *et al. J. Comput. Chem.* **2011**, *32*, 1456–1465.
[55] A. Klamt. *COSMO-RS: From Quantum Chemistry to Fluid PhaseThermodynamics and Drug Design*; Elsevier Science: Amsterdam, 2005.
[56] J. Tomasi *et al. Chem. Rev.* **2005**, *105*, 2999–3094.
[57] E. Runge and E. K. U. Gross. *Phys. Rev. Lett.* **1984**, *52*, 997–1000.
[58] M. E. Casida and M. Huix-Rotllant. *Annu. Rev. Phys. Chem.* **2012**, *63*, 287–323.
[59] N. T. Maitra. *J. Chem. Phys.* **2016**, *144*, 220901.
[60] S. J. A. van Gisbergen *et al. J. Chem. Phys.* **1995**, *103*, 9347–9354.
[61] C. A. Ullrich. *Time-Dependent Density-Functional Theory : Concepts and Applications*; Oxford Graduate Texts; OUP Oxford: Oxford, 2011.
[62] R. Car and M. Parrinello. *Phys. Rev. Lett.* **1985**, *55*, 2471–2474.
[63] D. Marx and J. Hutter. *Ab Initio Molecular Dynamics: Basic Theory and Advanced Methods*, 1 edition.; Cambridge University Press: Cambridge ; New York, 2009.
[64] J. K. Nørskov *et al. J. Phys. Chem. B* **2004**, *108*, 17886–17892.
[65] J. Rossmeisl *et al. J. Electroanal. Chem.* **2007**, *607*, 83–89.
[66] B. Ensing *et al. J. Phys. Chem. A* **2001**, *105*, 3300–3310.
[67] F. Costanzo and R. G. Della Valle. *J. Phys. Chem. B* **2008**, *112*, 12783–12789.
[68] M. Sprik and G. Ciccotti. *J. Chem. Phys.* **1998**, *109*, 7737–7744.
[69] W. K. den Otter and W. J. Briels. *J. Chem. Phys.* **1998**, *109*, 4139–4146.
[70] L. Bernasconi *et al. ACS Catal.* **2017**, *7*, 4018–4025.
[71] D. Frenkel and B. Smit. *Understanding Molecular Simulation: From Algorithms to Applications*, 2nd ed.; Academic Press: California, 2001.